FRONTIERS OF PHYSICS

RESEARCH ARTICLE
Volume 18 / Issue 3 / 33302 / 2023

Deterministic and replaceable transfer of silver flakes for microcavities

Tingting Wang[1,2], Zhihao Zang[1], Yuchen Gao[1], Kenji Watanabe[3], Takashi Taniguchi[4], Wei Bao[5], Yu Ye[1,2,6,†]

1 State Key Laboratory for Mesoscopic Physics and Frontiers Science Center for Nano-optoelectronics, School of Physics, Peking University, Beijing 100871, China
2 Collaborative Innovation Center of Quantum Matter, Beijing 100871, China
3 Research Center for Functional Materials, National Institute for Materials Science, 1-1 Namiki, Tsukuba, 305-0044, Japan
4 International Center for Materials Nanoarchitectonics, National Institute for Materials Science, 1-1 Namiki, Tsukuba, 305-0044, Japan
5 Electrical & Computer Engineering, University of Nebraska-Lincoln, Lincoln, NE 68588, USA
6 Yangtze Delta Institute of Optoelectronics, Peking University, Nantong 226010, China
Corresponding author. E-mail: †ye_yu@pku.edu.cn
Received October 7, 2022; accepted November 25, 2022

ABSTRACT

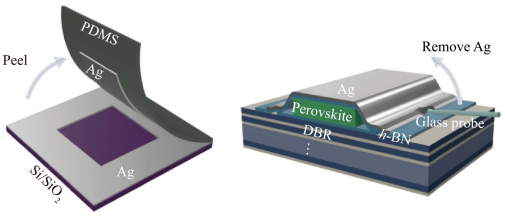

How to fabricate high-quality microcavities simply and at low cost without causing damage to environmentally sensitive active layers such as perovskites are crucial for the studies of exciton–polaritons, however, it remains challenging in the field of microcavity fabrication. Usually, once the top mirror is deposited, the detuning of the microcavity is fixed and there is no easy way to tune it. Here, we have developed a method for deterministically transferring silver mirrors, which is relatively simple and guarantees the active layer from damaging of high temperature, particle bombardment, etc., during the deposition of the top mirror. Furthermore, with the help of a glass probe, we demonstrate a replaceable silver transfer method to tune the detuning of the microcavity, thereby changing the coupling of photons and excitons therein. The developed deterministic and replaceable silver mirror transfer methods will provide the capability to fabricate high-quality and tunable microcavities and play an active role in the development of the exciton–polariton field.

Keywords silver, microcavity, transfer, perovskite

1 Introduction

Since the first experimental demonstration of the strong coupling of excitons and photons in AlGaAs quantum well microcavity [1], exciton–polariton related research has emerged one after another, covering multiple material systems including CdTe [2], wide bandgap semiconductors [3–5], two-dimensional (2D) materials [6–8], and perovskites [9–11], etc. Perovskites are a class of materials with a variety of excellent optical properties, such as tunable bandgap [12, 13], large exciton binding energy [14], large oscillator strength [15], high optical absorption coefficient [16], high optical gain [17], and strong emission anisotropy [18]. Recently, a large number of intriguing studies of exciton–polariton in perovskite microcavities have been reported [19–24], covering quantum, topological and other research fields. However, a key issue in the study of perovskite exciton–polariton is the simple and low-cost fabrication of high-quality microcavities without causing damage to active layers. To date, various approaches have been used to integrate perovskites into Fabry–Pérot microcavities, which typically consist of

Higher Education Press

https://doi.org/10.1007/s11467-022-1229-3

top and bottom mirrors and gain material embedded in them, where the bottom mirror is usually a distributed Bragg reflector (DBR), the top mirror is usually a DBR [25–27] or a silver mirror [28–30].

To form effective microcavities, perovskites are mechanically transferred [27] or grown directly [19] onto the substrates pre-deposited with DBRs that are optimized to possess high reflectivity in the desired wavelength range. Then, a dielectric layer for tuning the cavity length is deposited on the perovskite by coating or mechanical transfer. The top mirror deposition in the final step becomes the key to the fabrication of high-quality microcavities. Similarly, there are generally two ways to prepare top mirrors, namely evaporation and mechanical transfer. The evaporation method is applicable for the preparation of DBR and silver mirrors. Nonetheless, since perovskites are environmentally sensitive and vulnerable to high temperature and atomic bombardment damage during evaporation, the resulting rough surface may compromise the quality of the microcavity. Therefore, a more friendly method for preparing top mirrors for environmentally sensitive active materials such as perovskites is urgently needed. To meet this, by applying pressure and scratching on the DBR surface, 10–50 μm DBR flakes can be occasionally detached from the substrate and used as top mirrors to prepare high-quality microcavities [7, 31, 32]. However, the yield of separating the DBR from the substrate to obtain a flat surface is quite low, and moreover, particles would be produced to adhere to the DBR flakes during the scratching process, resulting in a large deviation of the cavity mode from the design.

To this end, we elaborate a simple and feasible method, the silver mirror deterministic transfer method, for the fabrication of tunable optical microcavities. The silver flakes can be transferred to any location on any substrate and fully maintain the flatness of the pristine silver film deposited directly on the Si/SiO_2 substrate. The transferred top silver mirror has excellent reflectivity and can be combined with the bottom DBR to fabricate high-quality bare or perovskite microcavities. Furthermore, the transferred silver mirror can be removed with the help of a glass probe, and after transferring a dielectric layer with a certain thickness, a new silver mirror can be deterministically transferred to adjust the total cavity length of the microcavity effectively. Our deterministic and replaceable high-quality top silver mirror transfer method provides an avenue to explore more interesting exciton–polariton phenomena.

2 Experimental section

Sample preparation. $CsPbBr_3$ microplates were synthesized on mica substrates in a home-built system via chemical vapor deposition method. The precursor powder (a mixture of CsBr and $PbBr_2$ with a molar ratio of 1:1) and the mica substrates (sequentially arranged at a distance of 17 cm to 22 cm from the precursor powders) were placed on a quartz boat, which was then inserted into a quartz tube placed in a single-zone furnace. The precursor powders were placed in the furnace heating center, while the substrates were placed downstream. The quartz tube was pumped to 40 mTorr and flushed with high-purity argon (Ar) gas ahead of heating. The growth was carried out at the optimized temperature (570 ℃) for 8 min with high-purity Ar gas at a flow rate of 25 sccm. The furnace was naturally cooled to room temperature under continuous Ar gas flow before the perovskites were collected. $CsPbBr_3$ microplates grown on mica substrates can be transferred to polydimethylsiloxane (PDMS) (GEL PAK, PF-17-X4) substrates for subsequent dry transfer to any substrates.

Atomic force microscope (AFM) characterization. The thicknesses and morphologies of $CsPbBr_3$ microplates were characterized by AFM (Cypher, Asylum Research) with tapping mode.

Optical characterization. Photoluminescence (PL) (absorption) experiments on $CsPbBr_3$ microplates were performed using the WITec alpha300 confocal innovation system with a 473 nm laser (broadband white light) as the excitation light source. Angle-resolved reflectivity and PL experiments were performed using a home-built optical setup. [24] The devices were kept in a liquid nitrogen cryostat (Janis ST-500) for low-temperature measurements. A broad-band white light source (Thorlabs SLS401) was used for angle-resolved reflectivity measurements as well as device imaging. A continuous wave laser (405 nm) was used as the excitation source for the angle-resolved PL measurements. The excitation light beam was focused (spot diameter of ~5 μm) by an objective (Zeiss Epiplan-Neofluar 50×/0.55 DIC M27). The emitted signals were collected by the same objective and sent into an Andor spectrometer (SR-500i-D2-R) equipped with gratings of 150, 600, and 1200 lines mm^{-1} and a Newton CCD (DU920P-BEX2-DD) of 256 × 1024 pixels.

3 Results and discussion

In order to visually demonstrate the deterministic silver transfer method, a schematic diagram of the transfer process and the corresponding optical microscope images are given in Figs. 1(a)–(f). Typically, due to the viscoelastic behavior of the elastomers, the adhesion between the solid objects (here silver films and perovskites) and the stamp (here PDMS is rate-sensitive) [33]. The key in the deterministic transfer process is the kinetics control of the adhesion and release of Ag flakes to and from the PDMS. First, a silver film of a certain thickness is evaporated onto a Si/SiO_2 substrate by the

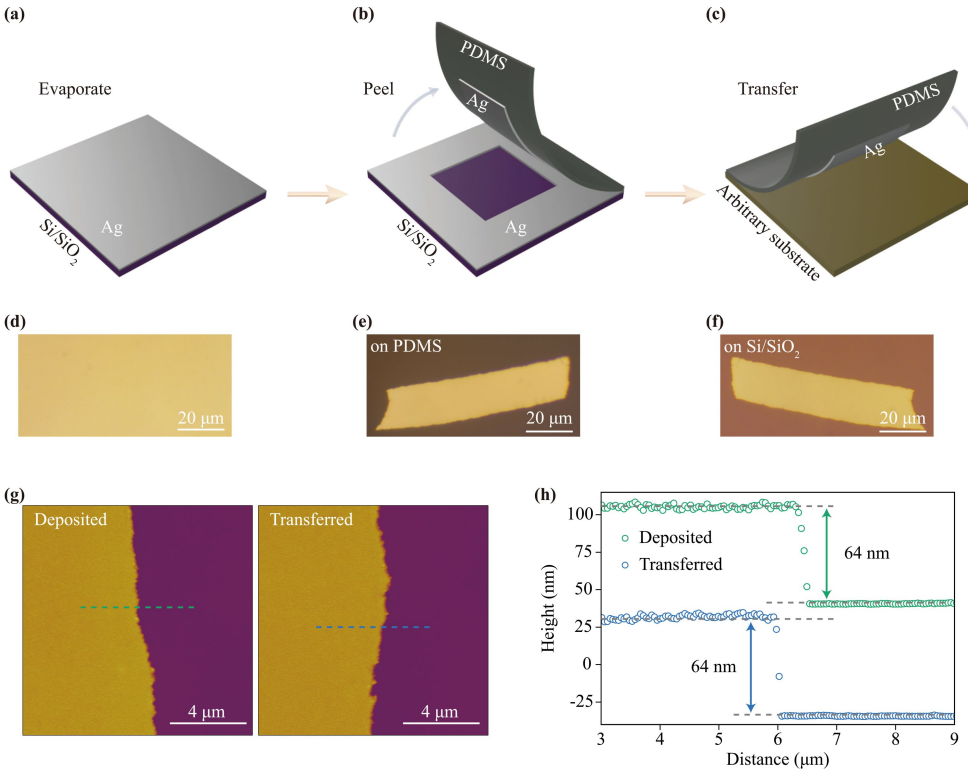

Fig. 1 Deterministic transfer and characterization of silver flakes. **(a–c)** Schematic illustration of the deterministic transfer method of silver flakes and **(d–f)** corresponding optical microscope images. **(g)** AFM height images of the deposited and transferred silver flakes. **(h)** Height line profiles of the silver flake before and after transfer along the dashed lines marked in (g).

widely-used electron beam evaporation (EBE) method [6, 28] [Figs. 1(a) and (d)]. Next, after attaching the silver-deposited substrate to a glass slide by double-side tape, we faced the silver film with the PDMS stamp adhered on another glass slide. Manually applying moderate pressure between the two sides for a few seconds makes the PDMS stamp conformal contact with the silver film. Pulling the PDMS stamp away from the silver surface at a peel speed high enough will lead to stamp adhesion to be strong enough to preferentially adhere the silver to the stamp surface, thus detaching the silver flakes from the initial Si/SiO_2 substrate to the PDMS stamp [Figs. 1(b) and (e)]. Since there is no adhesive layer between the silver film and Si/SiO_2 substrate, silver flakes are prone to be peeled from the substrate by another adhesive stamp. But metal films are known to be very soft and wrinkle or crack during the peeling process, which is fatal to the quality of the microcavity. Therefore, the peeling process should be carried out by pulling in the vertical direction quickly to reduce the lateral stress. This process is somewhat similar to the cleavage process of traditional 2D materials [34, 35], and will produce silver flakes of various sizes and shapes, including continuous silver flakes of hundreds of microns or even millimeters [Figs. S1 and S2 of the Supplementary Information (SI)]. Then, the appropriate silver flakes are selected carefully under the optical microscope. Finally, removing the PDMS stamp at a sufficiently low peel speed results in the selected silver flakes adhering preferentially to the target substrate and detaching from the PDMS stamp by the standard deterministic transfer method [36] [Figs. 1(c) and (f)]. Moreover, we found that as long as the thickness of the directly deposited silver is thick enough (thicker than 24 nm), a large number of large-sized silver flakes can be obtained through the deterministic silver transfer method (Fig. S2 of the SI). Similarly, using our deterministic transfer method, continuous gold flake up to ~200 μm × 200 μm was successfully transferred (Fig. S3 of the SI).

To verify the quality of the transferred silver flakes, we performed AFM characterization to determine the changes in the thickness and roughness of the silver film before and after transfer, which is of great implication for the quality of the microcavity [Figs. 1(g) and (h)]. For instance, a 64 nm silver film was directly evaporated onto a Si/SiO_2 substrate using EBE at a deposition rate of 1 Å/s. In order to exclude the influence of the substrate, we also transferred the silver flakes to the Si/SiO_2 substrate by the above method. The height images and height line profiles of the silver flakes before and after transfer show the same thickness of 64 nm [Figs. 1(g) and (h)]. In addition, the consistent surface roughness

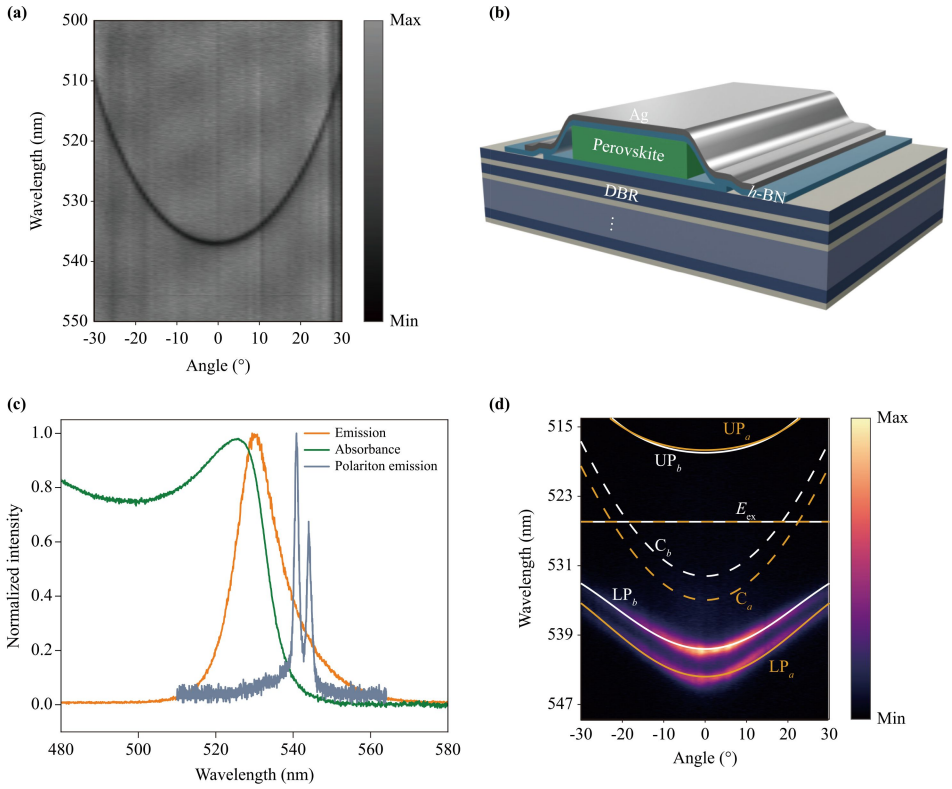

Fig. 2 High-quality microcavities composed of DBR and transferred silver flakes. **(a)** Angle-resolved reflectivity spectrum of the bare microcavity consisting of the bottom DBR, PMMA spacer layer and the transferred silver mirror. **(b)** Schematic cutaway view of a typical perovskite microcavity capped with an h-BN dielectric layer. **(c)** Room-temperature absorption (green trace), PL (orange trace) and polariton emission (at $k_{//} = 0$) (shadow blue trace) spectra of the $CsPbBr_3$ perovskite microplate. **(d)** Room-temperature angle-resolved PL spectrum of a $CsPbBr_3$ microcavity superimposed with the theoretical fitting curves. The marigold and white solid lines represent the upper (UP_a and UP_b) and lower (LP_a and LP_b) polariton branches, while the marigold and white dashed lines represent the uncoupled degenerate excitons (E_{ex}) and cavity photon modes (C_a and C_b) along the a-axis and b-axis, respectively.

before and after transfer ($R_a = 2.047$ nm for deposited silver flakes and $R_a = 1.975$ nm for transferred silver flakes, see Fig. S4 of the SI for more details) again proves that the quality of the transferred silver flakes remains intact.

For further investigations into the performance of the transferred silver flakes in the microcavities, which is one of the most important factors for studying exciton-polaritons, we constructed the microcavities based on the method of transferring the top silver mirror. The bare microcavity is composed of a bottom DBR, a dielectric layer, and a top transferred silver mirror. The bottom DBR consists of 14.5 pairs of Ta_2O_5/SiO_2 structures deposited on a silicon substrate by ion beam sputtering, with a carefully designed stop band centered at 532 nm. Then, a polymethyl methacrylate (PMMA) spacer layer was spin-coated onto the bottom DBR substrate at 3000 rpm for 1 min to meet the cavity resonance condition. After baking for 5 min on a hot plate at 150 ℃, an appropriate silver flake was transferred onto it. The angle-resolved reflectivity spectrum [Fig. 2(a)] show a distinct cavity resonance characteristic centered at 537.2 nm with a full width at half maximum (FWHM) of 0.96 nm and a passive cavity Q factor of ~560. It is worth mentioning that the Q factor is not only limited by the intrinsic absorption of the silver mirror, but also the roughness of the spacer layer. Therefore, when fabricating a microcavity based on $CsPbBr_3$ active layer, we used the atomically flat 2D material h-BN as the dielectric layer to tune the cavity length [Fig. 2(b)]. The cladding h-BN layer not only compensates the thickness of the microcavity, but also acts as the protective layer for the $CsPbBr_3$ microplate. The room-temperature optical properties of the $CsPbBr_3$ microplate shown in Fig. 2(c) indicate that the PL emission is centered at ~530 nm with a narrow FWHM of 13 nm (24 meV), while the absorption spectrum shows a strong excitonic peak centered at ~526 nm, suggesting the high quality and room-temperature-stable exciton properties of our $CsPbBr_3$ microplate.

To confirm whether our perovskite microcavity has entered the strong-coupling regime, we performed angle-resolved PL experiments at room temperature. In the angle-resolved PL map [Fig. 2(d)], it is difficult to identify

the upper polariton (UP) branches because of their large Rabi splittings and strong absorption above the bandgap, which is also very common in other perovskite microcavities [24, 27, 28]. Nonetheless, we can clearly distinguish the two lower polariton (LP) branches, LP_a and LP_b, which are attributed to the coupling between the microcavity and the $CsPbBr_3$ microplate along different crystalline axes due to its orthogonal birefringence effect [37], consistent with previous reports [20, 21, 24, 25]. It can be seen that as the angle increases, the curvature of the LP branches decreases, indicating that the system has entered the strong-coupling regime. Meanwhile, the theoretical fitting calculated by the coupled oscillator model is also shown in Fig. 2(d) (more details are shown in Note S1), where the solid lines represent the calculated polariton dispersions (UP_a, UP_b, LP_a, and LP_b), while dashed lines represent the uncoupled degenerate excitons (E_{ex}) and cavity photon modes (C_a and C_b). The fitting results are in good agreement with the experimental data, indicating the emergence of anti-crossing behavior, which again proves that the system is in the strong-coupling regime. From the fitting results, we can extract the cavity detuning ($\Delta = E_c - E_{ex}$) between exciton states and the cavity modes, and the Rabi splitting ($\hbar\Omega$) between the LP branches and the UP branches along the a-axis and b-axis, respectively, where $\Delta_a = E_{ca} - E_{ex} = -39.8$ meV, $\Delta_b = E_{cb} - E_{ex} = -27.7$ meV, $\hbar\Omega_a = 107.9$ meV, and $\hbar\Omega_b = 96.2$ meV. By fitting the linewidths of the LP branches (shadow blue trace in Fig. 2(c) and Fig. S5 of the SI), it is shown that the microcavity has a relatively high Q factor (~454 for LP_a, and ~420 for LP_b), which ensures the efficient strong coupling between excitons and the photons to form exciton–polaritons.

For a specific perovskite microplate, the dielectric layer needs to be added to meet the cavity resonance condition, and the required thickness can usually be estimated by the transfer matrix method or empirically. However, there is always a certain deviation between the actual situation and the simulation results, and designing a well-detuned microcavity is not an easy task. Generally speaking, whether it is a DBR or a silver mirror, once the top mirror is deposited, the detuning of the microcavity is determined and cannot be adjusted at will. To get rid of this predicament, we developed a replaceable transfer method of the silver mirrors to achieve the tuning of microcavity detuning with the aid of a glass probe immobilized on a three-dimensional (3D) translation stage. First, we fabricated a typical perovskite microcaivty of DBR/30 nm h-BN/178 nm $CsPbBr_3$/23 nm h-BN/30 nm Ag [see the optical microscope image in Fig. 3(d)]. To evaluate the detuning of the microcavity, that is, the coupling of excitons and photons, we measured its angle-resolved PL spectrum at 80 K, as shown in Fig. 3(h). Fitted by the coupled oscillator model (more details are shown in Note S1), the fabricated perovskite microcavity exhibits positive detuning ($\Delta_a = 37.0$ meV, $\Delta_b = 45.3$ meV), which means that the dispersion is more exciton-like, i.e., there is a higher proportion of excitons. More disappointingly, we simultaneously observe non-dispersed emission originating from uncoupled excitons due to the large positive detuning of the microcavity [38]. In this case, there is no good way to adjust the detuning of the microcavity before, and the best way is to make a new device. In Figs. 3(a)–(g), we show a schematic diagram and corresponding optical microscope images of the process of tuning the microcavity detuning by artificially adjusting the cavity length. First, insert the glass probe fixed on the 3D translation stage into one side of the top silver mirror, then move the translation stage so that the silver mirror will adhere to the glass probe and be peeled off from the device [Figs. 3(a) and (e)]. By comparing the optical images of the original device [Fig. 3(d)] and the device with the top silver mirror stripped off [Fig. 3(e)], we can delineate the outline of the stripped silver (light yellow dashed lines). Subsequently, a flake of h-BN with a specific thickness (here 25 nm) was transferred onto the device whose top silver mirror had been stripped away to tune the cavity length [Figs. 3(b) and (f)]. h-BN layers with different thicknesses will result in the distinct optical contrast. Therefore, by examining the optical images of the exfoliated h-BN layer on PDMS substrate (Fig. S6 of the SI), and the device before [Fig. 3(e)] and after [Fig. 3(f)] transfer of the additional h-BN layer, we can demarcate the h-BN layer transferred onto the device in Fig. 3(f), which was marked by the dark turquoise solid lines. Finally, a new silver mirror was transferred onto the device [Figs. 3(c) and (g)] to form a new microcavity. The angle-resolved PL spectrum of the new microcavity [Fig. 3(i)] is significantly different from that of the original device [Fig. 3(h)]. Based on the coupled oscillator model, we obtained a small cavity detuning, $\Delta_a = E_{ca} - E_{ex} = -4.7$ meV and $\Delta_b = E_{cb} - E_{ex} = 3.3$ meV, while the Rabi splitting $\hbar\Omega_a = 68.8$ meV and $\hbar\Omega_b = 60.8$ meV along the a-axis and b-axis, respectively. Moreover, contributions from excitonic and photonic components for each polariton branch can be calculated by the Hopfield coefficients (Fig. S7 of the SI), which helps us to intuitively demonstrate the role of the replaceable transfer method in tuning the coupling of excitons and photons. After the transfer of additional h-BN layer, the proportion of photonic components in the LP branches with different polarizations (especially LP_a) increases significantly, which indicates an increased overlap between the photon modes and the degenerate exciton mode. Likewise, the proportion of exciton components in the UP branches increases accordingly. Based on the calculation results of the Hopfield coefficients, we can show that the cavity length can be effectively adjusted by the replaceable silver transfer method, and thus the coupling of excitons and photons can be tuned.

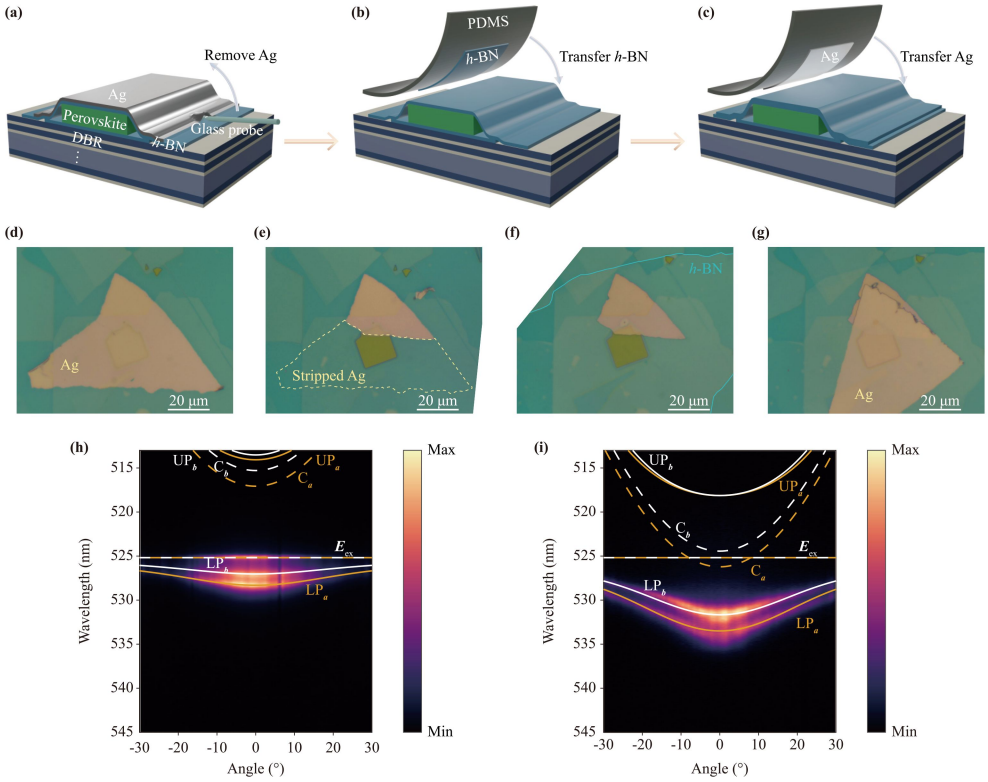

Fig. 3 Replaceable transfer of silver flakes and k-space dispersion of the tunable microcavity. **(a–c)** Schematic illustration, and **(d–g)** corresponding optical microscope images of the replaceable transfer process of silver flakes. The light yellow dashed lines in (e) demarcate the stripped Ag flake, while the dark turquoise solid lines in (f) demarcate the new transferred h-BN flake. **(h)** Angle-resolved PL spectrum recorded at 80 K of the as-prepared perovskite microcavity. **(i)** Angle-resolved PL spectrum recorded at 80 K of a new microcavity with a layer of h-BN added to the microcavity shown in (h) using the replaceable silver transfer method.

4 Conclusion

In summary, we systematically introduced a deterministic transfer method for silver mirror that can be widely used to fabricate top mirrors in microcavities without damaging the active layer. Meanwhile, we also developed a replaceable silver mirror transfer method for effectively tuning the microcavity length. In addition to technical interest, these silver mirror transfer methods open new perspectives for fabricating high-performance exciton-polariton devices to further explore novel exciton-polariton phenomena based not only on perovskites but also on other materials.

Electronic supplementary material Supplementary materials are available in the online version of this article at https://doi.org/10.1007/s11467-022-1229-3 and https://journal.hep.com.cn/fop/EN/10.1007/s11467-022-1229-3 and are accessible for authorized users.

Acknowledgements This work was supported by the National Natural Science Foundation of China (No. 61875001) and the Beijing Natural Science Foundation (No. JQ21018). W. B. acknowledge support from National Science Foundation (Award No. DMR-2143041). T. T. acknowledges support from the JSPS KAKENHI (Grant Nos. 19H05790 and 20H00354) and A3 Foresight by JSPS.

References

1. C. Weisbuch, M. Nishioka, A. Ishikawa, and Y. Arakawa, Observation of the coupled exciton-photon mode splitting in a semiconductor quantum microcavity, *Phys. Rev. Lett.* 69(23), 3314 (1992)
2. J. Kasprzak, M. Richard, S. Kundermann, A. Baas, P. Jeambrun, J. M. J. Keeling, F. M. Marchetti, M. H. Szymańska, R. André, J. L. Staehli, V. Savona, P. B. Littlewood, B. Deveaud, and L. S. Dang, Bose–Einstein condensation of exciton polaritons, *Nature* 443(7110), 409 (2006)
3. S. Christopoulos, G. B. H. von Högersthal, A. J. D. Grundy, P. G. Lagoudakis, A. V. Kavokin, J. J. Baumberg, G. Christmann, R. Butté, E. Feltin, J. F. Carlin, and N. Grandjean, Roomtemperature polariton lasing in semiconductor microcavities, *Phys. Rev. Lett.* 98(12), 126405 (2007)
4. F. Li, L. Orosz, O. Kamoun, S. Bouchoule, C. Brimont, P. Disseix, T. Guillet, X. Lafosse, M. Leroux, J. Leymarie, M. Mexis, M. Mihailovic, G. Patriarche, F. Réveret, D. Solnyshkov, J. Zuniga-Perez, and G.

Malpuech, From excitonic to photonic polariton condensate in a ZnO-based microcavity, *Phys. Rev. Lett.* 110(19), 196406 (2013)
5. C. Schneider, A. Rahimi-Iman, N. Y. Kim, J. Fischer, I. G. Savenko, M. Amthor, M. Lermer, A. Wolf, L. Worschech, V. D. Kulakovskii, I. A. Shelykh, M. Kamp, S. Reitzenstein, A. Forchel, Y. Yamamoto, and S. Höfling, An electrically pumped polariton laser, *Nature* 497(7449), 348 (2013)
6. L. Zhang, F. Wu, S. Hou, Z. Zhang, Y.-H. Chou, K. Watanabe, T. Taniguchi, S. R. Forrest, and H. Deng, Van der Waals heterostructure polaritons with moiré-induced nonlinearity, *Nature* 591(7848), 61 (2021)
7. N. Lundt, Ł. Dusanowski, E. Sedov, P. Stepanov, M. M. Glazov, S. Klembt, M. Klaas, J. Beierlein, Y. Qin, S. Tongay, M. Richard, A. V. Kavokin, S. Höfling, and C. Schneider, Optical valley Hall effect for highly valley-coherent exciton–polaritons in an atomically thin semiconductor, *Nat. Nanotechnol.* 14(8), 770 (2019)
8. J. Gu, B. Chakraborty, M. Khatoniar, and V. M. Menon, A room-temperature polariton light-emitting diode based on monolayer WS_2, *Nat. Nanotechnol.* 14(11), 1024 (2019)
9. R. Su, A. Fieramosca, Q. Zhang, H. S. Nguyen, E. Deleporte, Z. Chen, D. Sanvitto, T. C. Liew, and Q. Xiong, Perovskite semiconductors for room-temperature exciton-polaritonics, *Nat. Mater.* 20(10), 1315 (2021)
10. T. J. S. Evans, A. Schlaus, Y. Fu, X. Zhong, T. L. Atallah, M. S. Spencer, L. E. Brus, S. Jin, and X. Y. Zhu, Continuous-wave lasing in cesium lead bromide perovskite nanowires, *Adv. Opt. Mater.* 6(2), 1700982 (2018)
11. S. Zhang, Q. Shang, W. Du, J. Shi, Z. Wu, Y. Mi, J. Chen, F. Liu, Y. Li, M. Liu, Q. Zhang, and X. Liu, Strong exciton–photon coupling in hybrid inorganic–organic perovskite micro/nanowires, *Adv. Opt. Mater.* 6(2), 1701032 (2018)
12. Q. Zhang, R. Su, X. Liu, J. Xing, T. C. Sum, and Q. Xiong, High-quality whisperinggallery-mode lasing from cesium lead halide perovskite nanoplatelets, *Adv. Funct. Mater.* 26(34), 6238 (2016)
13. L. Protesescu, S. Yakunin, M. I. Bodnarchuk, F. Krieg, R. Caputo, C. H. Hendon, R. X. Yang, A. Walsh, and M. V. Kovalenko, Nanocrystals of cesium lead halide perovskites ($CsPbX_3$, X = Cl, Br, and I): Novel optoelectronic materials showing bright emission with wide color gamut, *Nano Lett.* 15(6), 3692 (2015)
14. J. C. Blancon, H. Tsai, W. Nie, C. C. Stoumpos, L. Pedesseau, C. Katan, M. Kepenekian, C. M. M. Soe, K. Appavoo, M. Y. Sfeir, S. Tretiak, P. M. Ajayan, M. G. Kanatzidis, J. Even, J. J. Crochet, and A. D. Mohite, Extremely efficient internal exciton dissociation through edge states in layered 2D perovskites, *Science* 355(6331), 1288 (2017)
15. A. Fieramosca, L. Polimeno, V. Ardizzone, L. De Marco, M. Pugliese, V. Maiorano, M. De Giorgi, L. Dominici, G. Gigli, D. Gerace, D. Ballarini, and D. Sanvitto, Two-dimensional hybrid perovskites sustaining strong polariton interactions at room temperature, *Sci. Adv.* 5(5), eaav9967 (2019)
16. M. A. Green, A. Ho-Baillie, and H. J. Snaith, The emergence of perovskite solar cells, *Nat. Photonics* 8(7), 506 (2014)
17. S. Yakunin, L. Protesescu, F. Krieg, M. I. Bodnarchuk, G. Nedelcu, M. Humer, G. De Luca, M. Fiebig, W. Heiss, and M. V. Kovalenko, Low-threshold amplified spontaneous emission and lasing from colloidal nanocrystals of caesium lead halide perovskites, *Nat. Commun.* 6, 8056 (2015)
18. Y. Gao, L. Zhao, Q. Shang, Y. Zhong, Z. Liu, J. Chen, Z. Zhang, J. Shi, W. Du, Y. Zhang, S. Chen, P. Gao, X. Liu, X. Wang, and Q. Zhang, Ultrathin $CsPbX_3$ nanowire arrays with strong emission anisotropy, *Adv. Mater.* 30(31), 1801805 (2018)
19. L. Polimeno, G. Lerario, M. De Giorgi, L. De Marco, L. Dominici, F. Todisco, A. Coriolano, V. Ardizzone, M. Pugliese, C. T. Prontera, V. Maiorano, A. Moliterni, C. Giannini, V. Olieric, G. Gigli, D. Ballarini, Q. Xiong, A. Fieramosca, D. D. Solnyshkov, G. Malpuech, and D. Sanvitto, Tuning of the Berry curvature in 2D perovskite polaritons, *Nat. Nanotechnol.* 16(12), 1349 (2021)
20. R. Su, S. Ghosh, J. Wang, S. Liu, C. Diederichs, T. C. Liew, and Q. Xiong, Observation of exciton polariton condensation in a perovskite lattice at room temperature, *Nat. Phys.* 16(3), 301 (2020)
21. R. Su, S. Ghosh, T. C. Liew, and Q. Xiong, Optical switching of topological phase in a perovskite polariton lattice, *Sci. Adv.* 7(21), eabf8049 (2021)
22. R. Su, J. Wang, J. Zhao, J. Xing, W. Zhao, C. Diederichs, T. C. Liew, and Q. Xiong, Room temperature long-range coherent exciton–polariton condensate flow in lead halide perovskites, *Sci. Adv.* 4(10), eaau0244 (2018)
23. R. J. Tao, K. Peng, L. Haeberlé, Q. W. Li, D. F. Jin, G. R. Fleming, S. Kéna-Cohen, X. Zhang, and W. Bao, Halide perovskites enable polaritonic XY spin Hamiltonian at room temperature, *Nat. Mater.* 21, 761 (2022)
24. T. Wang, Z. Zang, Y. Gao, C. Lyu, P. Gu, Y. Yao, K. Peng, K. Watanabe, T. Taniguchi, X. Liu, Y. Gao, W. Bao, and Y. Ye, Electrically pumped polarized exciton–polaritons in a halide perovskite microcavity, *Nano Lett.* 22(13), 5175 (2022)
25. M. S. Spencer, Y. Fu, A. P. Schlaus, D. Hwang, Y. Dai, M. D. Smith, D. R. Gamelin, and X. Y. Zhu, Spin-orbit-coupled exciton–polariton condensates in lead halide perovskites, *Sci. Adv.* 7(49), eabj7667 (2021)
26. Y. Li, X. Ma, X. Zhai, M. Gao, H. Dai, S. Schumacher, and T. Gao, Manipulating polariton condensates by Rashba–Dresselhaus coupling at room temperature, *Nat. Commun.* 13, 1 (2022)
27. R. Su, C. Diederichs, J. Wang, T. C. H. Liew, J. Zhao, S. Liu, W. Xu, Z. Chen, and Q. Xiong, Room-temperature polariton lasing in all-inorganic perovskite nanoplatelets, *Nano Lett.* 17(6), 3982 (2017)
28. W. Bao, X. Liu, F. Xue, F. Zheng, R. Tao, S. Wang, Y. Xia, M. Zhao, J. Kim, S. Yang, Q. Li, Y. Wang, Y. Wang, L. W. Wang, A. H. MacDonald, and X. Zhang, Observation of Rydberg exciton polaritons and their condensate in a perovskite cavity, *Proc. Natl. Acad. Sci. USA* 116(41), 20274 (2019)
29. L. Polimeno, A. Fieramosca, G. Lerario, M. Cinquino,

M. De Giorgi, D. Ballarini, F. Todisco, L. Dominici, V. Ardizzone, M. Pugliese, C. T. Prontera, V. Maiorano, G. Gigli, L. De Marco, and D. Sanvitto, Observation of two thresholds leading to polariton condensation in 2D hybrid perovskites, *Adv. Opt. Mater.* 8(16), 2000176 (2020)

30. A. Brehier, R. Parashkov, J. S. Lauret, and E. Deleporte, Strong exciton–photon coupling in a microcavity containing layered perovskite semiconductors, *Appl. Phys. Lett.* 89(17), 171110 (2006)
31. C. Rupprecht, N. Lundt, M. Wurdack, P. Stepanov, E. Estrecho, M. Richard, E. A. Ostrovskaya, S. H¨ofling, and C. Schneider, Micro-mechanical assembly and characterization of high-quality Fabry–Pérot microcavities for the integration of two-dimensional materials, *Appl. Phys. Lett.* 118(10), 103103 (2021)
32. C. Rupprecht, M. Klaas, H. Knopf, T. Taniguchi, K. Watanabe, Y. Qin, S. Tongay, S. Schröder, F. Eilenberger, S. Höfling, and C. Schneider, Demonstration of a polariton step potential by local variation of light-matter coupling in a van-der-Waals heterostructure, *Opt. Express* 28(13), 18649 (2020)
33. M. A. Meitl, Z. T. Zhu, V. Kumar, K. J. Lee, X. Feng, Y. Y. Huang, I. Adesida, R. G. Nuzzo, and J. A. Rogers, Transfer printing by kinetic control of adhesion to an elastomeric stamp, *Nat. Mater.* 5(1), 33 (2006)
34. M. Yi and Z. Shen, A review on mechanical exfoliation for the scalable production of graphene, *J. Mater. Chem. A* 3(22), 11700 (2015)
35. F. Liu, Mechanical exfoliation of large area 2D materials from vdW crystals, *Prog. Surf. Sci.* 96(2), 100626 (2021)
36. A. Castellanos-Gomez, M. Buscema, R. Molenaar, V. Singh, L. Janssen, H. S. Van Der Zant, and G. A. Steele, Deterministic transfer of two-dimensional materials by all-dry viscoelastic stamping, *2D Mater.* 1, 011002 (2014)
37. M. Rodová, J. Brožek, K. Knížek, and K. Nitsch, Phase transitions in ternary caesium lead bromide, *J. Therm. Anal. Calorim.* 71(2), 667 (2003)
38. R. Jayaprakash, F. G. Kalaitzakis, G. Christmann, K. Tsagaraki, M. Hocevar, B. Gayral, E. Monroy, and N. T. Pelekanos, Ultra-low threshold polariton lasing at room temperature in a GaN membrane microcavity with a zero-dimensional trap, *Sci. Rep.* 7, 5542 (2017)